

Semi-collapse of turbulent fountains in stratified media and the mechanisms to control their dynamics

Luis G. Sarasúa^{1*}, Daniel Freire Caporale^{1*}, Nicasio Barrere²
and Arturo C. Martí^{1*}

^{1*}Instituto de Física, Universidad de la República, Uruguay.

^{2*}Centro Universitario del Este, Universidad de la República,
Uruguay.

*Corresponding author(s). E-mail(s): sarasua@fisica.edu.uy;

dfreire@fisica.edu.uy; marti@fisica.edu.uy;

Contributing authors: nbarrere@fisica.edu.uy;

Abstract

Turbulent fountains are widespread natural phenomena with numerous industrial applications. Extensive research has focused on the temporal evolution and maximum height of these fountains, as well as their dependence on Reynolds and Froude numbers. However, the minimum height of the surrounding ambient fluid, which is removed by the fountain due to the entrainment effect, has received little attention. In this study, we investigate the dependence of this minimum height on the characteristics of the fountain and demonstrate how to control it. Our findings present important implications for technological applications of turbulent fountains, particularly in contaminant withdrawal. We discuss the potential of our results to improve the efficiency of such applications.

Keywords: turbulent fountain, stratified media, semi-collapse, fluid control, contaminant withdrawal

1 Introduction

A fountain is a vertical buoyant jet in which the buoyancy force and the jet's initial velocity act in opposite directions. On the other hand, the flow is a plume if the buoyancy force acts in the same direction as the jet velocity. Fountains and plumes are frequently encountered in nature and technical applications. Since the fluid dynamics in stratified media presents problems of considerable interest across several fields, turbulent fountains and plumes in stratified media have been the research subject for decades [1–13]. In particular, the behaviour of the pollutants ejected into the atmosphere is of great interest due to the effects these emissions produce on human health and nature in general [14]. Although air pollution is caused by emissions from different kind of sources, fountain flows often appear in the process of contaminant ejection as a consequence of the use of stacks [14]. The evolution of the contaminants in the atmosphere is usually described by models like the Gaussian plume model, which depends on parameters that are determined by empirical relations. Although these models are proven to be useful, these do not allow the study of effects of variations in the characteristics of the flow at the source.

Fountain dynamics in stratified media can be outlined as follows. At an initial stage, the fountain decelerates due to the opposing buoyancy force and the entrainment of ambient fluid reaching a maximum height at which the vertical momentum is zero. Then the flow reverses direction and falls as an annular plume around the fountain core. Depending on the initial fluxes of momentum and buoyancy and the initial stratification profile, the fountain spreads outwards at a non-zero spreading height, above the source level, or the flow collapses, i.e., it falls to the source or ground level (the terrain).

Some aspects of the turbulent fountains in the quasi-steady regime can be described using the well-known MTT model proposed by Morton, Taylor and Turner [5–7], which describe the evolution of volume, momentum, and buoyancy fluxes in fountains. In this model, it is assumed that the horizontal velocity at which the ambient fluid enters the fountain is proportional to the vertical velocity in the fountain, with a proportionality coefficient called the entrainment coefficient. Although successful in predicting the evolution in a uniform ambient and the maximum height in plumes [2], the MTT model do not describe the dynamics after the vertical velocity reverses its direction. Bloomfield and Kerr [8] proposed that the spreading height can be obtained by matching it to the height where the fluid density of the environment is equal to the fluid density at the maximum height. This condition is used to estimate h_m and h_{sp} combining different models. This approach may be considered a first-order because it does not take into account the mixing between fountain and ambient fluid in the downflow that occurs after the fountain reverses its direction.

Some years later, Kaminski et al. [15] developed an expression for the entrainment coefficient depending on three parameters that can be experimentally determined. A comparison between the predictions based on this

expression and the experimental data was given in [16] for the case of a homogeneous medium. Mehaddi et al. [17] studied fountains in stratified environments and obtained expression for the maximum height. However, the spreading behaviour of the fountain was not considered in this investigation. Papanicolaou et al. [18] conducted an experimental study on the collapse and spreading of turbulent fountains and performed a comparison with those obtained in [8]. As various authors have pointed out [19–21], to assume a constant entrainment coefficient is an approximation due to its dependence on the turbulence intensity, and, as a consequence, it can vary with the rise of the fountain. Recently, Sarasua et al. [22] proposed a model that generalizes the model of Morton et al. to determine the dependence of the maximum and the spreading height with the parameters involved. This model determines the critical conditions for the collapse of the fountain, i.e., when the jet falls to the source level, using a parameter that measures the mixing of the jet with the environment along the downflow.

Despite these contributions, a study of the dependence of the minimal height of the spreading flow, here referred to as *critical height* with the parameters controlling the flow, is not available yet. For configurations where the collapse regime does not occur, the critical height determines whether the fluid removed by the entrainment mechanism and later deviated to the spreading cloud will be again in contact with the ground or not.

This study focuses on a detailed analysis of the flow structure of turbulent fountains, specifically, the maximum, spreading, and critical heights, using fully validated numerical simulations. We investigate several configurations of turbulence levels and introduce a novel parameter, the dimensionless *lightness*, which depends on the temperature difference between the impinging fountain and the ambient fluid at the inlet. Our findings are abridged in a diagram that results a powerful tool for the design of technological applications of turbulent fountains in stratified media. Based on this diagram, we propose strategies to modify the fountain conditions and control its subsequent dynamics, particularly, the final regime developed. Our work presents significant implications for practical applications of turbulent fountains in the industry.

The structure of this work is as follows. First, in Section 2, we provide a detailed description of our case study. In Section 3, we analyse the characteristics of the domain, the experimental setup and procedure, the implemented numerical simulations, and their full validation with the experimental results. Subsequently, in Section 4, we present and analyse the results obtained. Specifically, we introduce a dimensionless parameter, the “lightness”, report on the height variation with the relevant parameters, and summarise the results in a diagram aimed at controlling the characteristic fountain dynamics heights. Finally, in Section 5, we draw our conclusions.

2 Problem description

In engineering applications involving pollutant emissions, it is of importance to warranty that the generated spreading flux does not fall below certain level. Therefore, in addition to the maximum and spreading heights, h_m and h_{sp} , respectively, we defined a third characteristic height, the *critical height*, h_c ($h_c \leq h_{sp}$), as the minimum height that the spreading cloud reaches, which develops after the flow reversion falling and stabilisation at h_{sp} . For instance, if $h_c \sim 0$ a potential hazard will occur since fluid ejected falls back to the ground.

Three different regimes, sketched in Fig. 1, can be developed by the fountain. First, there is the case in which the extracted fluid does not come into contact with the ground surface again, so-called the non-collapse regime, discriminated by $h_{sp} > 0$ and $h_c > 0$ (Fig. 1a). Second, the semi-collapse regime, Fig. 1b, in which, although the front of the spreading flow does not make contact with the ground ($h_{sp} > 0$), its lower edge does ($h_c = 0$), that is, the ejected flow comes back into contact with the ground. Finally, the third case, Fig. 1c is the collapse regime, in which $h_{sp} = 0$ and $h_c = 0$.

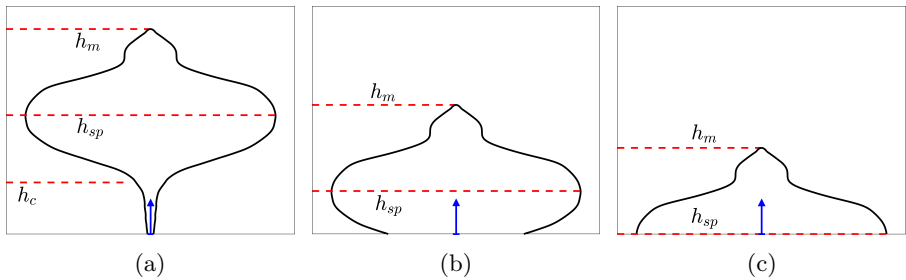


Fig. 1: The three possible dynamics of the developed fountain at developed stages: (a) no collapse when $h_{sp} > 0$ and $h_c > 0$; (b) semi-collapse when $h_{sp} > 0$ and $h_c = 0$; (c) collapse when $h_{sp} = 0$ (and so it does $h_c = 0$). Black lines correspond to the fountain contour and the upward-pointing blue arrows indicate the fountain inflow (the gravity points downwards).

For engineering applications devoted to the removal of contaminated air from the vicinity of the ground (lower ambient strata) it is crucial to elucidate the fountain's conditions at the entrance that guarantee the non-collapse regime. In the present work, we aimed at finding the subsequent flow regime based on the flow conditions at the inlet. For this purpose, we performed numerical simulations, previously validated with experiments, where the temperature profile of the environment stratification was kept constant and each simulation case was performed for a given value of T_{in} and the turbulence level.

3 Problem configuration

The experimental setup was designed based on scaling a technological application called Selective Inverted Sink (SIS)[23], which represents a remarkable breakthrough utilising turbulent fountains to mitigate frost damage in agriculture under radiation frost conditions.

This section is organized as follows. First, we present detailed experimental measurements conducted in the laboratory in Section 3.1. Secondly, we explain the computational simulations performed in Section 3.2. Finally, in Section 3.3, we compare the experimental and numerical results to validate the latter calculations.

3.1 Experimental Setup

We present laboratory experiments carried out in a rectangular acrylic tank of dimensions 40 cm \times 40 cm \times 50 cm in width (x) \times depth (y) \times height (z) filled with water. The temperature of the ambient fluid was arranged to have a linear profile, with $T_{cold} = 15$ °C at the lower boundary ($z = 0$) and $T_{hot} = 27.5$ °C at the upper boundary ($z = 50$ cm), leading to a temperature gradient of 25 °C·m⁻¹. Hence, the initial temperature profile of the quiescent ambient fluid was given by $T(t = 0, z) = \partial_z T \cdot z + T_{cold}$.

To establish a stable stratification, we followed a meticulous procedure. Starting from the lowermost layers of water, we inserted a 1 kW electrical resistance and gradually heated the fluid while monitoring its temperature using a thermocouple. Once the target temperature was reached (depending on the vertical position of the resistance), we carefully moved the resistance upwards to the next fluid layer, repeating this procedure until we reached the highest layer of fluid at $z = 50$ cm. The bottom and top plates of the container were controlled using cooler and heater, respectively, which were regulated by relays. We insulated the tank using 10 cm deep expanded polystyrene panels and monitored the temperature gradient using thermocouples installed every 10 cm along two vertical edges of the tank. By following this meticulous procedure, we successfully established a quiescent ambient fluid with a stable linear vertical stratification in temperature. Fig. 2 shows a typical temperature profile obtained at the end of this procedure.

The fountain was generated by injecting water vertically at $T_{in} = 15$ °C, at a stable flow rate of $\dot{q}_{in} = 5.5$ cm³/s, through a circular nozzle with a diameter of $D = 8$ mm, positioned at the center of the tank bottom plate. Figures 5(a)–(c) displays experimental images for the grid configuration obtained using the dye tracer technique.

We investigated the flow using two methods: dye (tracer) visualization and Digital Particle Image Velocimetry (DPIV) [24–26]. The former method allowed us to track the evolution of the inflow (colored fluid) as its dynamics evolved, and mixing and diffusion occurred. The latter enabled us to determine the velocity fields of the seeded fluids. To capture the velocity fields, we illuminated the fluid with a 500 mW green LASER sheet of 2 mm thickness

and captured images using a CMOS camera at 4 fps. We processed the images using the open-source package OpenPIV [27]. We performed DPIV experiments in both free and grid configurations. In the grid configuration, we placed an 80-mesh screen with a wire diameter of 0.18 mm transversally at the jet inlet to generate different degrees of turbulence [28]. To ensure the reliability of the results, the experiments were conducted with 2-3 repetitions for each configuration and technique. Figures 7 (a) and (c) present an example of the experimentally measured horizontal and vertical components, respectively, of the velocity field for the free configuration at 60 s.

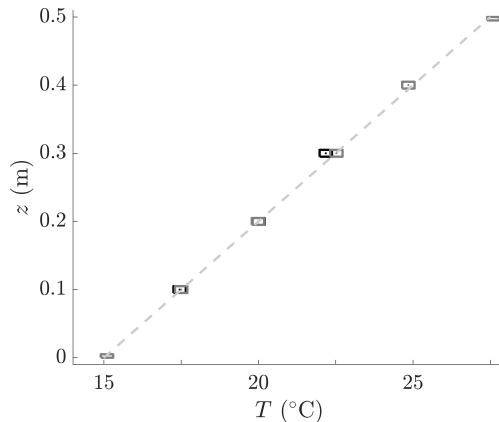


Fig. 2: Typical temperature stratification profile observed experimentally before injecting the fountain into the system at an inlet temperature of $T_{in} = 15^\circ\text{C}$. Rectangles indicate experimental measurements with their corresponding uncertainties while the dashed line represents a linear fit. The two sets of rectangles (black and gray) correspond to two vertical container edges where thermocouples were installed every 10 cm.

In this work, we present both experimental and numerical studies on the flow of confined turbulent fountains in a stratified medium. To extrapolate the results for studying the efficiency of the SIS device, the measurement period was approximately 120 s, during which the characteristic heights became stabilized, and no significant recirculation velocities were observed in the vicinity of the container walls.

3.2 Computer Simulations Setup

We conducted extensive numerical simulations using the open-source package `caffa3d.MBRi` [29, 30] that implements the Finite Volume Method [31]. The fluid properties in our simulations were set to those of pure water, consistent with the experimental conditions. The domain dimensions and the inlet flow rate in our simulations were set to match those of the experiments described

in Sec. 3.1. The calculations used a time step of 0.05 s, and the computational domain was discretized as represented in Fig. 3 into 8×10^6 hexahedral cells, ensuring mesh independence by utilizing both a coarser and a finer grid with similar results.

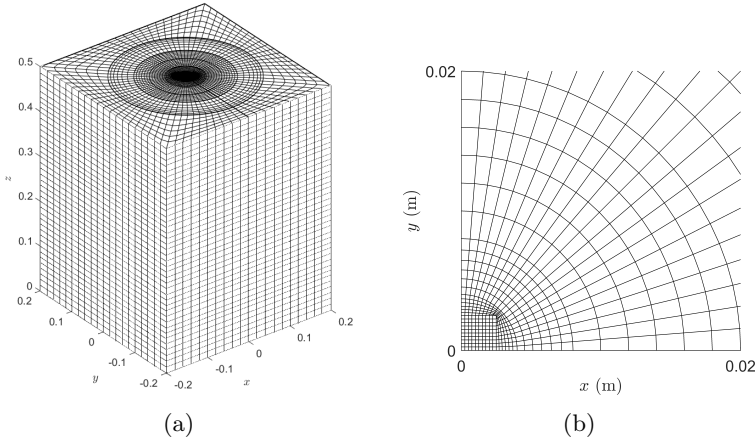


Fig. 3: Distribution of domain-discretization cells shown from two different perspectives: (a) a perspective view and (b) a projection onto the (x, y) -plane.

Turbulence was modeled using the Smagorinsky large-eddy model [32], where the constant factor in the subgrid viscosity μ_{sgs} was set to $C_S = 0.16$. In order to replicate the behavior of the dye tracer observed in our experiments, a passive scalar field represented by ϕ was employed to indicate the concentration of dye in the fluid flow. Initially, ϕ was assigned a value of 1 at the fountain inlet and 0 elsewhere. Subsequently, the interplay of advection, mixing, and diffusion caused ϕ to vary between 0 and 1 over time within the computational domain. A representative example of the computed flows is depicted in Fig. 4.

As explained in the previous section, the turbulence intensity of the fountain at the inlet was controlled during the experiments by means of a grid positioned at the entrance. For the numerical simulations, this turbulence intensity was synthetically adjusted by introducing random fluctuations, denoted as $\mathbf{u}' = (u_x, u_y, u_z)$, to the mean velocity at the inlet, i.e., $\mathbf{U}_{\text{in}} = \langle \mathbf{U}_{\text{in}} \rangle + \mathbf{u}'$. At every simulation time step, u_x , u_y , and u_z were randomly assigned to each cell located along the inlet port, with a uniform distribution. For a given turbulence level $u'/U \in [0, 1]$, u_x , u_y , and u_z are set randomly at each cell of the inlet port and at every time step, so that $u_i/U \in [-u'/U, +u'/U]$, where $\langle u_i \rangle = 0$ for $i \in x, y, z$. We employed a uniform distribution to generate such random fluctuations in our calculations. For a given turbulence level $u'/U \in [0, 1]$, u_x , u_y , and u_z are set randomly at each cell of the inlet port and at every time step, so that $u_i/U \in [-u'/U, +u'/U]$, where $\langle u_i \rangle = 0$ for $i \in x, y, z$. We employed a uniform distribution to generate such

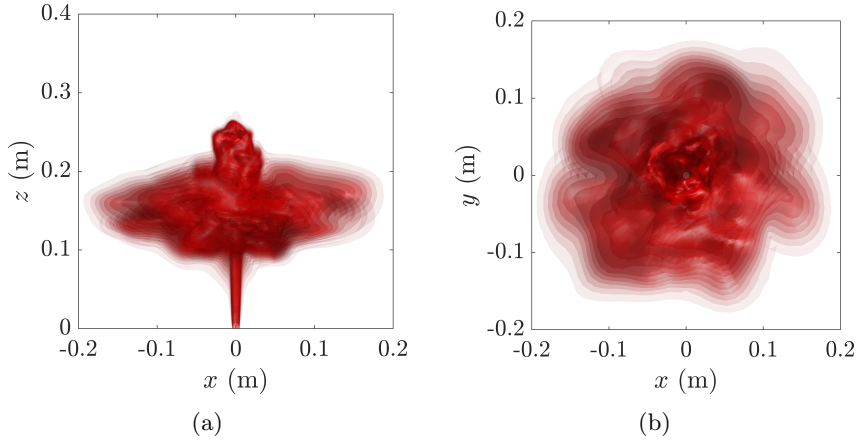
8 *Semi-collapse of turbulent fountains..*

Fig. 4: Snapshots of the passive tracer field ϕ : lateral, (x, z) -plane, (a) and top perspective (x, y) -plane (b). Parameter values: $t = 100$ s, $\xi = 0$, $u'/U = 1$.

random fluctuations in our calculations. Assuming a constant inlet flow rate \dot{q}_{in} , we set the velocity at each cell within the inlet as $\mathbf{U}_{in} = (u_x, u_y, U + u_z)$, where $U = \frac{\dot{q}_{in}}{\pi D^2/4}$ is the average vertical velocity at every cell within the inlet boundary condition. We conducted simulations at turbulence levels of $u'/U = 0, 1, 2, 4, 10$, and 20%. By adjusting the turbulence intensity, we were able to replicate the experimental results for the free and grid flow configurations with turbulence intensity values of $u'/U = 1$ and 20%, respectively. These results are shown in Section 3.3.

3.3 Validation of Computer Simulations

As detailed in Sec. 3.1, we studied two configurations, the free and grid configurations, at $\xi = 0$. We employed two different measurement techniques, dye tracer and DPIV, although not simultaneously, and repeated each experiment 2-3 times. Similarly, as explained in Sec.3.2, we computed the passive tracer and velocity fields throughout the numerical simulations. We validated the computer simulation results by comparing them with the corresponding experimental results.

Figs. 5(d)–(f) shows the numerical results of ϕ for the ($\xi = 0$, $u'/U = 20\%$) configuration. As can be easily observed by comparison with Figs. 5(a)–(c), this configuration corresponds to the experimental grid configuration. The same holds if we compare the results of the free experimental configuration with those of the numerical ($\xi = 0$, $u'/U = 1\%$) configuration.

One of the most significant analyses is the comparison of the time evolution of the characteristic heights h_m and h_{sp} between experiments and numerical simulations (further details about the height measurements are given in Sec. 4.1). This analysis is presented in Fig.6. It confirms that the evolution of the fountain for the free configuration follows the same pattern as the numerical

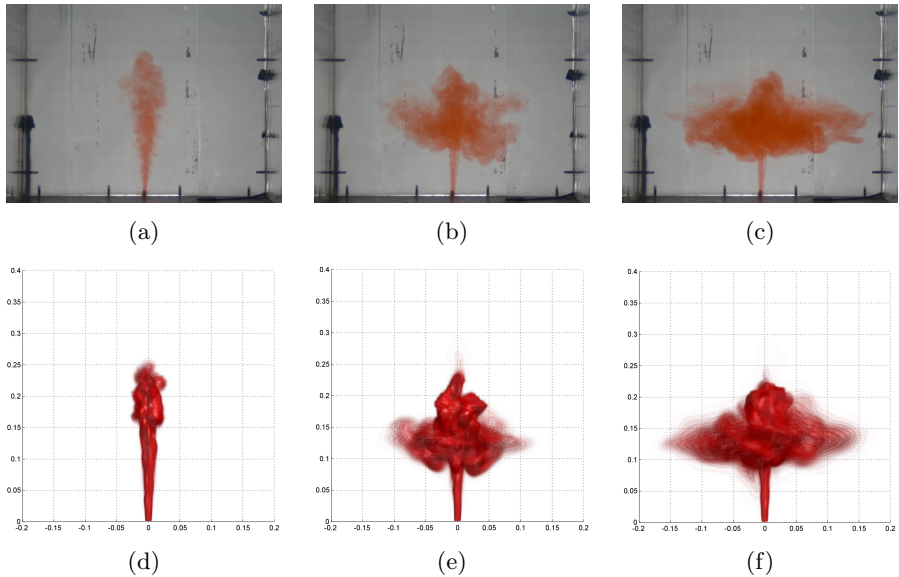


Fig. 5: Experimental (first row) and numerical (second row) results obtained using the red tracer technique for the grid and ($\xi = 0$, $u'/U = 20\%$) configuration. Panels (a) and (d) correspond to $t = 5$ s, (b) and (e) to 30 s, and (c) and (f) to 65 s. The lower boundary of the first-row images represents the full width of the container (40 cm), which serves as the length-scale reference.

simulation for $u'/U = 1\%$, while the grid configuration follows the numerical simulation for $u'/U = 20\%$. The comparison of the characteristic heights provides an essential basis for understanding the physical processes involved in the fountain's evolution and helps to validate the numerical simulations.

Finally, we compared the two-dimensional velocity fields measured experimentally at the plane $y = 0$ using the DPIV technique with the results obtained from the numerical simulations. The corresponding results for the free (grid) experimental configuration were found to be in excellent agreement with the simulations for $\xi = 0$ and $u'/U = 1\%$ (20%). For instance, Fig. 7 shows the velocity components obtained experimentally for the free experimental configuration at $t = 60$ s, and we compare the results with the simulations performed for $\xi = 0$ and $u'/U = 1\%$ at the same time.

Based on the present analysis, we conclude that the simulations are in good agreement with the experimental results, and therefore, we can proceed with parameter sweeps across the proposed range.

4 Results

After validating the numerical results, simulations were conducted to explore the effect of varying values of the temperature of the fountain at the inlet and

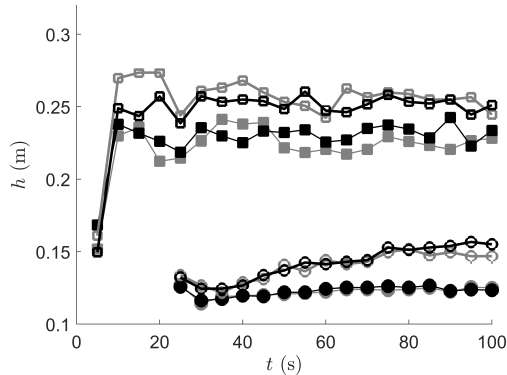


Fig. 6: The experimental and numerical results for the maximum and spreading heights of the fountain are shown. The black (grey) markers correspond to the experimental (numerical) results. The square (circular) markers correspond to h_m (h_{sp}), and the hollow (filled) markers correspond to the free (grid) configuration with $\xi = 0$ and $u'/U = 1\%$ (20%).

turbulence intensity. Specifically, simulations were performed for all combinations of $T_{in} = 4, 5, 7.5, 10, 12.5,$ and 15°C and $u'/U = 0, 1, 2, 4, 10,$ and 20% , respectively. To quantify our findings, we introduce the dimensionless parameter ξ . This parameter is defined as $\xi = -\text{Fr}^{-2}$, where Fr represents the Froude number at the inlet, which can be expressed as $\text{Fr} = U/\sqrt{gD\frac{\rho_{in}-\rho_{00}}{\rho_{00}}}$, where ρ_{in} is the density of the fountain at the inlet, $\rho_0(z)$ represents the initial density field of the stratified ambient fluid, and $\rho_{00} = \rho_0(z = 0)$ denotes the density of water at the given temperature. The aforementioned densities were computed based on the fluid temperature and tabulated properties of water. Note that ξ grows monotonically with T_{in} since $\rho_{in} \leq \rho_{00}$, as shown in Tab. 1. For this reason, we refer to ξ as the *lightness* of the fountain.

Table 1: Fountain lightness, ξ , as a function of the inlet temperature, T_{in} .

T_{in} ($^\circ\text{C}$)	4.0	5.0	6.0	7.5	10.0	12.5	15.0
ξ ($\times 10^{-3}$)	-6.1	-6.0	-5.9	-5.5	-4.3	-2.5	0

Our study aimed to analyze the flow characteristics resulting from different combinations of two control parameters: the lightness and turbulence intensity of the fountain. In Fig. 8, we present numerical results for the passive tracer field with a turbulence intensity of 20% and three distinct lightness values, leading to the three different regimes described earlier.

In this section, we organize the discussion as follows: in Sec. 4.1, we provide details of the procedure used to obtain the characteristic heights of the flow from the numerical simulations. In Sec. 4.2, we present the results and corresponding analysis. Finally, in Sec. 4.3, we examine the impact of the

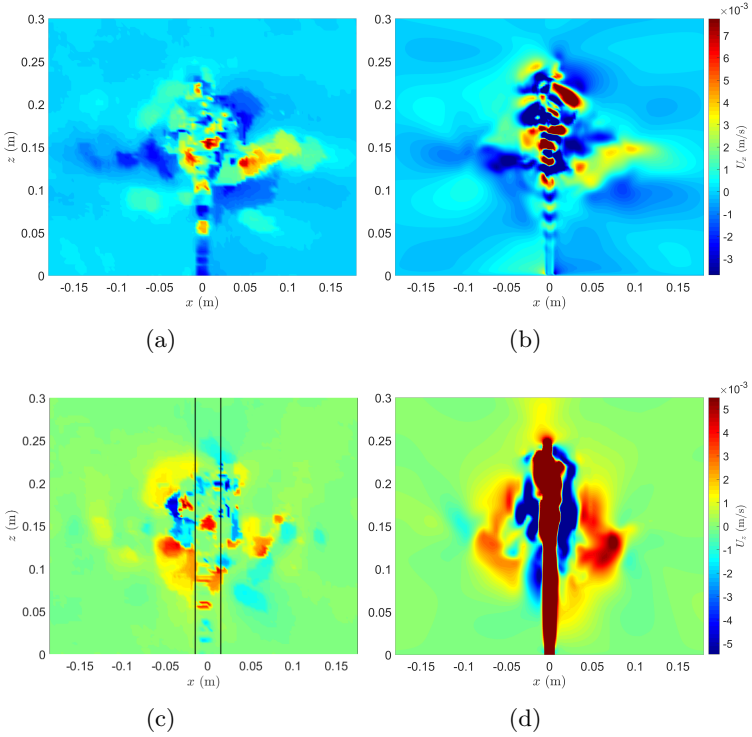


Fig. 7: Horizontal (top row) and vertical (bottom row) velocity components at 60 s obtained using the DPIV technique for the free experimental and numerical ($u'/U = 1\%$) configurations. The first column corresponds to the experimental data, and the second column corresponds to the numerical simulations. The color scales are consistent within each row. The central jet is not visible in (c) due to the limitations of the CMOS digital camera used. Therefore, comparison between (c) and (d) must be made outside the fountain axis region, delimited by the two vertical black lines in (c).

fountain-developed dynamics on the effectiveness of its technological applications for contaminant removal, specifically, the Selective Inverted Sink (SIS) device.

4.1 Characteristic heights measurement

Given the complexity of the three-dimensional flow the measurement of the characteristic heights h_m , h_{sp} and h_c requires the proper processing of the numerical results. In all cases, the calculation is based on the passive scalar tracer concentration field ϕ . Nevertheless, we separate the strategy for the calculation of h_m and h_{sp} from the used for h_c . We analysed the concentration field ϕ of the passive scalar tracer during the fully developed flow stage, i.e.,

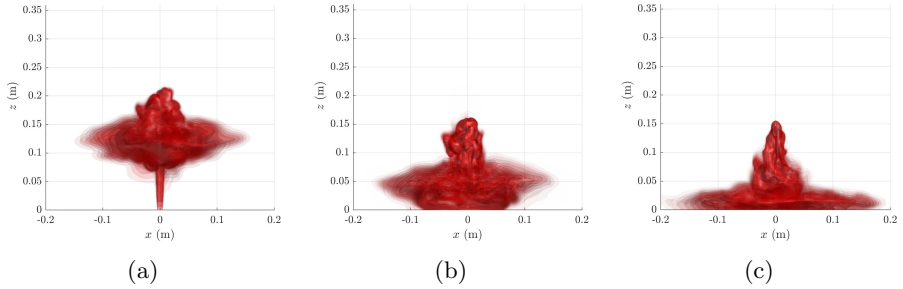


Fig. 8: Passive tracer field for the three different regimes of the fountain dynamics observed: (a) no-collapse ($\xi = 0$), (b) semi-collapse ($\xi = -4.3 \times 10^{-3}$), and (c) collapse ($\xi = -6.1 \times 10^{-3}$). Parameter value: $u'/U = 20\%$.

after the values of h_m and h_{sp} reached nearly constant values. To define the contour of the developed fountain at each time $\mathcal{C}(t)$, we initially established a threshold ϕ_{tol} in an arbitrary manner. After some experiments, we found $\phi_{tol} = 0.01$ sharply defines the fountain contour. The described procedure applied to the tracer field from Fig. 4 leads to the results shown in Fig. 9. On one hand, we define $h_m(t)$ as the height of the top of $\mathcal{C}(t)$. On the other hand, after approximating the front of the spreading cloud, at the maximum radial position of $\mathcal{C}(t)$, with a horizontal parabola, we obtain $h_{sp}(t)$ as the height of the extrema of such a parabola. Finally, for a given configuration of lightness and turbulence level of the fountain ($\xi, u'/U$), h_m and h_{sp} are defined as the mean of $h_m(t)$ and $h_{sp}(t)$, respectively, for $t = 100, 105, 110, 115$ and 120 s. The dimensionless maximum and spreading heights, defined as $h_m^* = h_m/D$ and $h_{sp}^* = h_{sp}/D$, are shown in Figs. 10 and 11, respectively.

To obtain h_c , we took into account that the grid is composed of horizontal layers of cells. For each height, z_c , we computed $\phi_{min}(z_c)$ as the minimum of ϕ for locations away from the uprising fountain, i.e., beyond an arbitrary given cut-off radial distance from the fountain axis. Such radial distance was chosen as three times the radius of the inlet. For a given tolerance value for tracer concentration, ϕ_{tol} , we define

$$h_c(\phi_{tol}) = \min\{z_c, \text{ such that } \phi_{min}(z_c) \geq \phi_{tol}\} \quad (1)$$

and dimensionless critical height as $h_c^* = h_c/D$.

4.2 Results for the characteristic heights

The behavior of the characteristic heights as a function of the parameter values is crucial to determine the occurrence of the semi-collapse regime. In Figs. 10 and 11 we show the maximum and spreading heights as a function of the lightness and turbulence level of the fountain. We observe, in agreement with previous works [22, 33] that, for a given lightness level, both heights decrease monotonically with the turbulence level. While for low fountain lightness, the

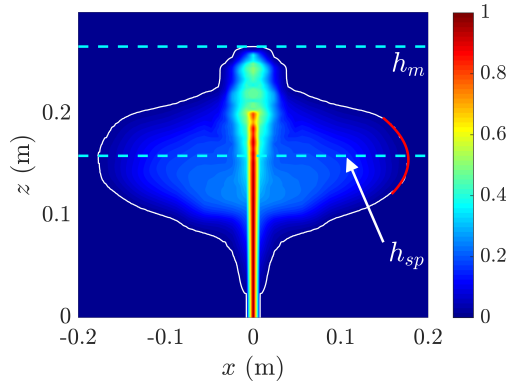


Fig. 9: Colour map of the azimuthal average of the tracer concentration (ϕ) at $t = 110$ s for the configuration $\xi = 0$, $u'/U = 1\%$. The solid white line represents the contour of the averaged fountain \mathcal{C} . The top of such a contour defines h_m (top cyan dashed horizontal line); meanwhile, the height of the extrema of the red line, corresponding to the parabola that fits the spreading cloud front, corresponds to h_{sp} (bottom cyan dashed horizontal line).

three critical heights are zero, non-intuitive results are observed for high lightness levels of the fountain. In such a case, the critical height is not monotonous but presents a maximum for a certain turbulence level instead. To check that the results do not depend on the tolerance chosen for the passive concentration, in Figs. 12, 13 and 14 we show the results for three different values. We conclude from these figures that the qualitative dependence is very similar for the three values displayed.

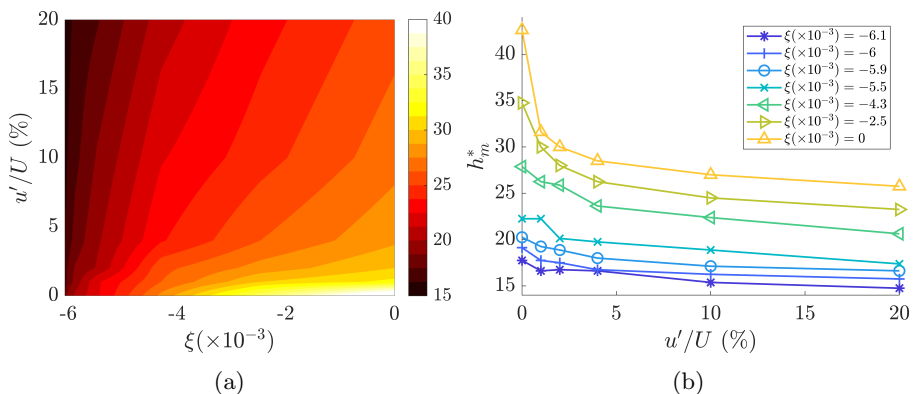


Fig. 10: Dimensionless maximum height, h_m^* , as a function of its lightness, ξ , and turbulence level, u'/U : (a) heatmap; (b) level curves.

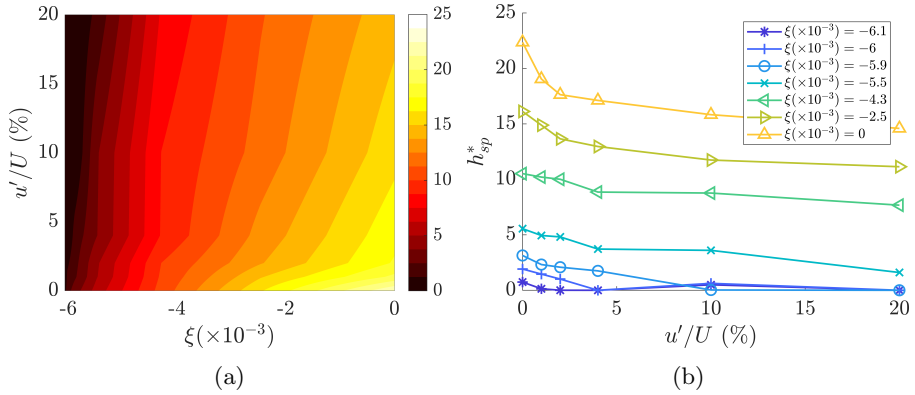


Fig. 11: Dimensionless spreading height, h_{sp}^* , as a function of its lightness, ξ , and turbulence level, u'/U : (a) heatmap; (b) level curves.

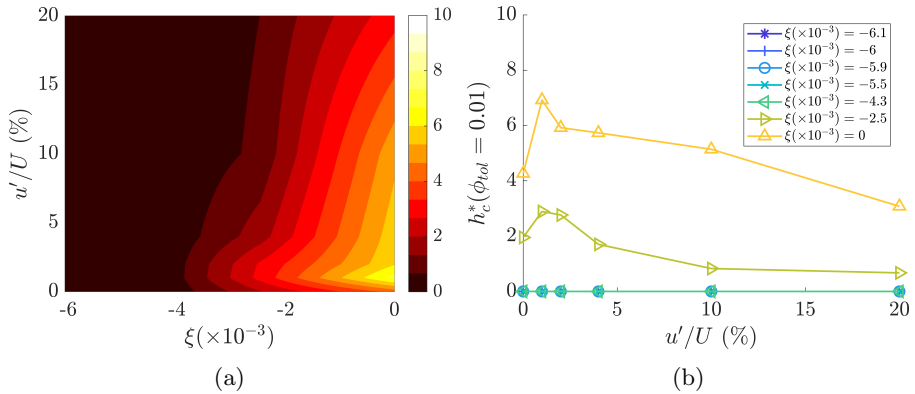


Fig. 12: Dimensionless critical height, h_c^* , for a tracer concentration tolerance of $\phi_{tol} = 0.01$: (a) heatmap; (b) level curves.

To summarise the previous results, in the diagram of Fig. 15, we condense the results from the previous graphs. Such a diagram divides the configuration space lightness – turbulence level in three regions, each corresponding to a different behaviour of the fountain at developed stages: collapse when $h_{sp} \leq 0$, semi-collapse when $h_{sp} > 0$ and $h_c > 0$ and no-collapse. Different boundaries between no-collapse and semi-collapse regions are determined depending on the value of ϕ_{tol} . For non-small values of ϕ_{tol} (meaning a high tolerance to the contaminant), the critical fountain lightness value for the occurrence of semi-collapse is weakly dependent on the turbulence level (e.g., line $\phi_{tol} = 0.20$ in Fig. 15). However, for small values of ϕ_{tol} (e.g., $\phi_{tol} = 0.01$), such a boundary is not monotonous. It can be observed from the diagram that the desirable non-collapse regime is more stable at a certain low fluctuation level

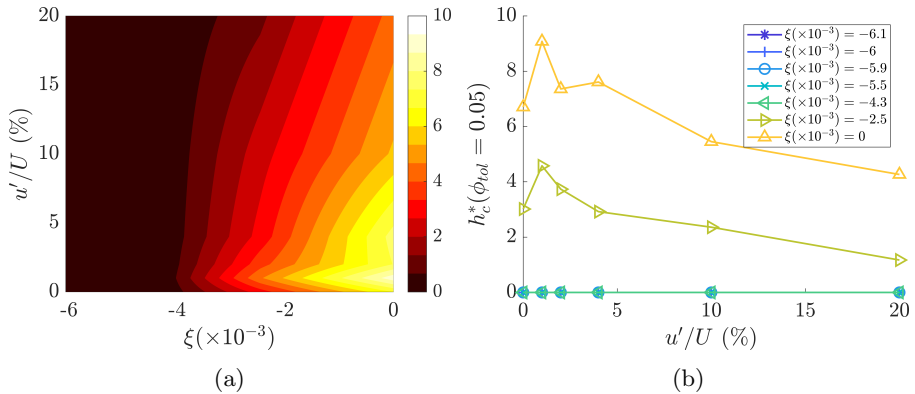


Fig. 13: Dimensionless critical height, h_c^* , for a tracer concentration tolerance of $\phi_{tol} = 0.05$: (a) heatmap; (b) level curves.

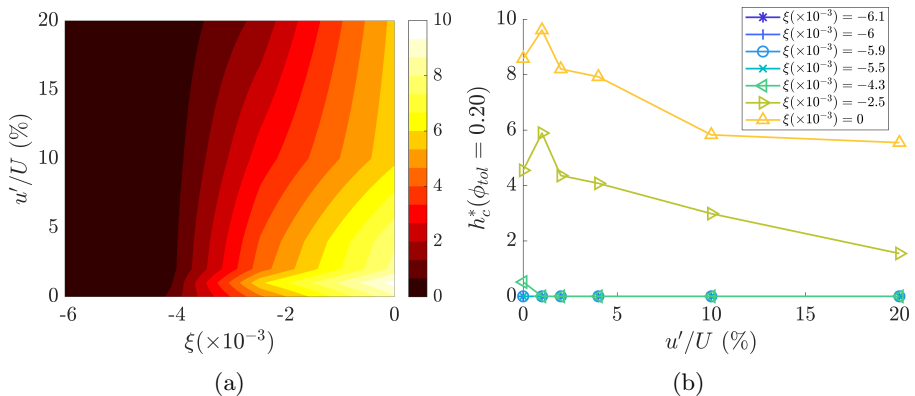


Fig. 14: Dimensionless critical height, h_c^* , for a tracer concentration tolerance of $\phi_{tol} = 0.20$: (a) heatmap; (b) level curves.

since the no-collapse region is broader there. In addition, from this figure, it is observed the no-collapse region boundary for $\phi_{tol} = 0.01$ presents a minimum with respect to the turbulence level. From Fig. 15, the such minimum is located about the coordinates $(\xi = -3.7 \times 10^{-3}, u'/U = 1\%)$. For technical applications of fountains for the removal of contaminants, as explained in Sec. 4.3, such behaviour means that starting from semi-collapse configurations whose lightness level is $\xi > -3.7 \times 10^{-3}$, transition to the desired no-collapse regime can be induced by decreasing the turbulence level of the fountain if $u'/U > 1\%$, or increasing such turbulence level if $u'/U < 1\%$. The latter is a surprising result and is a key contribution of the present work, not reported before to the best of the authors' knowledge.

Meanwhile, regarding the lightness level of the fountain for a given turbulence level, the transition from a semi-collapse to a no-collapse regime can only be done by increasing the fountain's lightness, i.e., increasing the fountain temperature T_{in} .

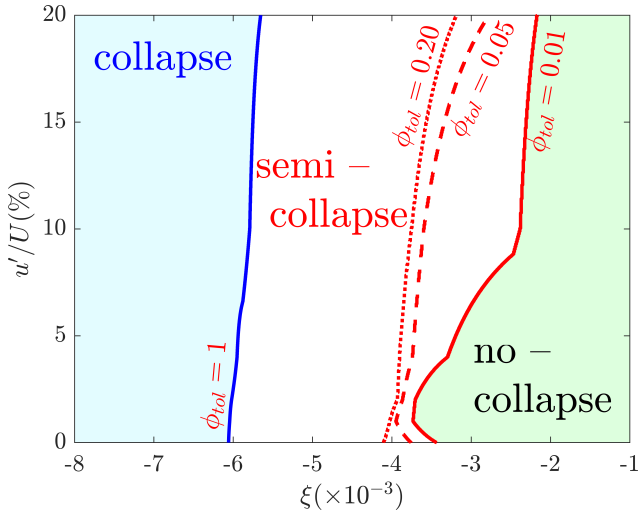


Fig. 15: Developed regimes in terms of its lightness, ξ , and turbulence level, u'/U : collapse (light-blue), semi-collapse (white), and no-collapse (green). The red curves delimiting the semi-collapse region depend on the concentration thresholds as indicated in the legends.

4.3 Effectiveness on the contaminant removal

In addition to this primary application, the SIS device offers various other notable features and applications [34]. The device operates at a lightness level of $\xi = 0$ by selectively removing the lower strata of air under thermal inversion stratification conditions. The average diameter of the SIS is approximately 3 – 4 m and it is designed to protect the surrounding area by redirecting the removed air above a critical height of $h_c \geq 6 - 8$ m, which corresponds to a height of at least $2D$ [34]. From Figs. 12 to 14), we corroborate that it is achieved only for $\xi = 0$. In fact, during operation, the spreading height in the field is about 50 m, which is in excellent agreement with our results. Moreover, from Fig. 12, it is also feasible for $\xi = -2.5 \times 10^{-3}$ and $u'/U \leq 2\%$, meaning that if the fountain is colder than the air close to the ground, the air would still be clean below $2D$ if the turbulence intensity is small.

A key aspect is the percentage of the terrain that is affected by contaminants under semi-collapse conditions. For a given value of ϕ_{tol} , we define the contaminated terrain percentage, $CTP(\phi_{tol})$, as the total area of the plane at the ground ($z = 0$) where $\phi \geq \phi_{tol}$ divided by the total area. The results of

CTP for $\phi_{tol} = 0.01$ and 0.20 are shown in Fig. 16a and 16b, respectively. In case of not so strict requirements, for instance, $CTP \leq 10\%$, from Fig. 16, we conclude that every configuration with $\xi \geq -4.3 \times 10^{-3}$ (i.e., $T_{in} \geq 10$ °C) is safe, no matter the level of turbulence.

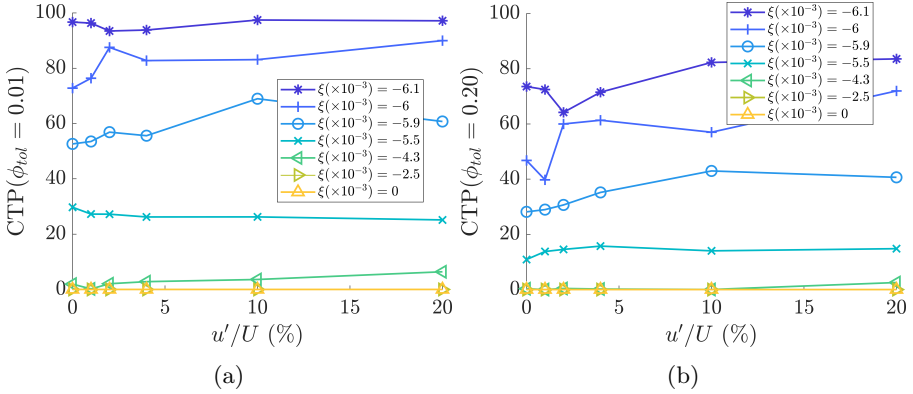


Fig. 16: Contaminated terrain percentage (CTP) as a function of the turbulence level, u'/U , for different values of the lightness ξ . Tolerance values of the passive scalar concentration: (a) $\phi_{tol} = 0.01$ and (b) $\phi_{tol} = 0.20$.

5 Final remarks

In this study, we investigated the collapse of turbulent fountains, focusing on the impact of the turbulence level and a characteristic parameter known as lightness. This parameter is defined by the temperature difference between the fountain and the surrounding ambient fluid at the fountain inlet (ground) level. We identified three distinct regimes based on the spreading height, h_{sp} , and the minimum or *critical* height, h_c : collapse regime for $h_{sp} \leq 0$; semi-collapse regime for $h_{sp} > 0$ and $h_c > 0$; and no-collapse regime for $h_{sp} > 0$. To effectively monitor and measure the characteristic heights of the flow, we introduced a passive scalar tracer concentration field into the inflow. The determination of the critical height h_c is a delicate process that relies heavily on the selected tracer tolerance level.

Our results are consistent with previous research indicating that an increase in turbulence level reduces both h_m and h_{sp} . However, the dependence of h_c on the turbulence level is non-monotonic and strongly influenced by the ϕ_{tol} . For large enough values of ϕ_{tol} , the critical lightness value for the occurrence of semi-collapse is weakly dependent on the turbulence level. Remarkable, for lower values of ϕ_{tol} , such as $\phi_{tol} = 0.01$, the critical height h_c exhibits a non-monotonic behavior. As a result, the no-collapse regime is more stable at a

certain low fluctuation level, as shown in Fig. 15. This allows for a transition from the semi-collapse regime to the no-collapse regime by increasing the turbulence level. Additionally, two possible transitions from a semi-collapse to a no-collapse configuration are possible under certain conditions, either by decreasing or increasing the turbulence level. However, to observe such a transition the fountain lightness must be increased.

Finally, we applied our analysis to evaluate the effectiveness of turbulent fountains in removing pollutants modelled by a the scalar field concentration. Of particular interest was the semi-collapse scenario, where we examined the percentage of contaminated terrain where $\phi \geq \phi_{tol}$. Our findings revealed that regardless of ϕ_{tol} , the proportion of contaminated terrain remained below 10% for $\xi \geq -4.3 \times 10^{-3}$ (i.e., $T_{in} \geq 10.0$ °C), independent of the turbulence level. Thus, our analysis provides a powerful tool for enhancing the efficiency of technological applications, such as the SIS device.

Data availability

The data that support the findings of this study are available from the corresponding author upon reasonable request.

Declarations

Competing interests: The authors have no competing interests or other interests that might be perceived to influence the results and/or discussion reported in this paper.

Authors' contributions: Luis G. Sarasúa conceived the numerical experiment, analysed and discussed the results, and contributed to manuscript writing. Daniel Freire Caporale performed the laboratory and numerical experiments, analysed the results, prepared the figures, and contributed to manuscript writing. Nicasio Barrere contributed to the numerical experiment and analysis of the results. Arturo C. Martí participated in the experiment's design, contributed to the analysis of the results, prepared the final version, and reviewed the manuscript.

Funding: The received partial funding by PEDECIBA (MEC, UdelaR, Uruguay) and grant Fisica Nolineal (ID 722) Programa Grupos I+D CSIC 2018 (UdelaR, Uruguay).

References

- [1] Woods, A.W.: Turbulent plumes in nature. *Annual Review of Fluid Mechanics* **42**(1), 391–412 (2010). <https://doi.org/10.1146/annurev-fluid-121108-145430>
- [2] Kaye, N.B.: Turbulent plumes in stratified environments: A review of recent work. *ATMOSPHERE-OCEAN* **46**(4), 433–441 (2008). <https://doi.org/10.3137/ao.460404>

- [3] Hunt, G.R., Burridge, H.C.: Fountains in industry and nature. *Annual Review of Fluid Mechanics* **47**(1), 195–220 (2015). <https://doi.org/10.1146/annurev-fluid-010313-141311>
- [4] Turner, J.S.: Buoyant plumes and thermals. *Annual Review of Fluid Mechanics* **1**(1), 29–44 (1969). <https://doi.org/10.1146/annurev.fl.01.010169.000333>
- [5] Morton, B.R., Taylor, G.I., Turner, J.S.: Turbulent gravitational convection from maintained and instantaneous sources. *Proceedings of the Royal Society of London. Series A. Mathematical and Physical Sciences* **234**(1196), 1–23 (1956). <https://doi.org/10.1098/rspa.1956.0011>
- [6] Morton, B.R.: Forced plumes. *Journal of Fluid Mechanics* **5**(01), 151 (1959). <https://doi.org/10.1017/s002211205900012x>
- [7] Morton, B.R., Middleton, J.: Scale diagrams for forced plumes. *Journal of Fluid Mechanics* **58**(01), 165 (1973). <https://doi.org/10.1017/s002211207300220x>
- [8] BLOOMFIELD, L.J., KERR, R.C.: Turbulent fountains in a stratified fluid. *Journal of Fluid Mechanics* **358**, 335–356 (1998). <https://doi.org/10.1017/s0022112097008252>
- [9] BLOOMFIELD, L.J., KERR, R.C.: Turbulent fountains in a confined stratified environment. *Journal of Fluid Mechanics* **389**, 27–54 (1999). <https://doi.org/10.1017/s0022112099004772>
- [10] Richards, T.S., Aubourg, Q., Sutherland, B.R.: Radial intrusions from turbulent plumes in uniform stratification. *Physics of Fluids* **26**(3), 036602 (2014). <https://doi.org/10.1063/1.4869119>
- [11] Camassa, R., Lin, Z., McLaughlin, R.M., Mertens, K., Tzou, C., Walsh, J., White, B.: Optimal mixing of buoyant jets and plumes in stratified fluids: theory and experiments. *Journal of Fluid Mechanics* **790**, 71–103 (2016). <https://doi.org/10.1017/jfm.2015.720>
- [12] Carroll, D., Sutherland, D.A., Shroyer, E.L., Nash, J.D., Catania, G.A., Stearns, L.A.: Modeling turbulent subglacial meltwater plumes: Implications for fjord-scale buoyancy-driven circulation. *Journal of Physical Oceanography* **45**(8), 2169–2185 (2015). <https://doi.org/10.1175/jpo-d-15-0033.1>
- [13] Ezhova, E., Cenedese, C., Brandt, L.: Interaction between a vertical turbulent jet and a thermocline. *Journal of Physical Oceanography* **46**(11), 3415–3437 (2016). <https://doi.org/10.1175/jpo-d-16-0035.1>

- [14] Vallero, D.A.: *Fundamentals of Air Pollution*. Academic press, Oxford (2014)
- [15] Kaminski, E., Tait, S., Carazzo, G.: Turbulent entrainment in jets with arbitrary buoyancy. *Journal of Fluid Mechanics* **526**, 361–376 (2005)
- [16] Carazzo, G., Kaminski, E., Tait, S.: The rise and fall of turbulent fountains: a new model for improved quantitative predictions. *Journal of fluid mechanics* **657**, 265–284 (2010)
- [17] Mehaddi, R., Vauquelin, O., Candelier, F.: Analytical solutions for turbulent boussinesq fountains in a linearly stratified environment. *Journal of Fluid Mechanics* **691**, 487–497 (2011). <https://doi.org/10.1017/jfm.2011.487>
- [18] Papanicolaou, P., Stamoulis, G.: Spreading of buoyant jets and fountains in a calm, linearly density-stratified fluid. *Environmental hydraulics*, 123–128 (2010)
- [19] Turner, J.S., Turner, J.S.: *Buoyancy Effects in Fluids*. Cambridge university press, Cambridge (1979)
- [20] Telford, J.: The convective mechanism in clear air. *Journal of Atmospheric Sciences* **23**(6), 652–666 (1966)
- [21] van Reeuwijk, M., Craske, J.: Energy-consistent entrainment relations for jets and plumes. *Journal of Fluid Mechanics* **782**, 333–355 (2015)
- [22] Sarasua, L., Freire, D., Cabeza, C., Marti, A.C.: Spreading height and critical conditions for the collapse of turbulent fountains in stratified media. *Physics of Fluids* **33**(1), 015106 (2021)
- [23] SIS Technologies. <https://frostprotection.com/index.php?lang=en-us>
- [24] Westerweel, J.: *Fundamentals of digital particle image velocimetry*. Measurement science and technology **8**(12), 1379 (1997)
- [25] Gui, L., Merzkirch, W.: Generating arbitrarily sized interrogation windows for correlation-based analysis of particle image velocimetry recordings. *Experiments in fluids* **24**(1), 66–69 (1998)
- [26] Adrian, R.J., Westerweel, J.: *Particle Image Velocimetry* vol. 30. Cambridge university press, Cambridge (2011)
- [27] Ben-Gida, H., Gurka, R., Liberzon, A.: Openpiv-matlab—an open-source software for particle image velocimetry; test case: Birds’ aerodynamics. *SoftwareX* **12**, 100585 (2020)

- [28] Freire, D., Cabeza, C., Pauletti, S., Sarasúa, G., Bove, I., Usera, G., Martí, A.C.: Effect of turbulent fluctuations on the behaviour of fountains in stratified environments. In: *Journal of Physics: Conference Series*, vol. 246, p. 012015 (2010). IOP Publishing
- [29] Usera, G., Vernet, A., Ferré, J.: A parallel block-structured finite volume method for flows in complex geometry with sliding interfaces. *Flow, Turbulence and Combustion* **81**(2), 471 (2008)
- [30] Mendina, M., Draper, M., Soares, A.P.K., Narancio, G., Usera, G.: A general purpose parallel block structured open source incompressible flow solver. *Cluster Computing* **17**(2), 231–241 (2014)
- [31] Ferziger, J.H., Perić, M., Street, R.L.: Finite volume methods. In: *Computational Methods for Fluid Dynamics*, pp. 81–110. Springer, Cham (2020)
- [32] Smagorinsky, J.: General circulation experiments with the primitive equations: I. the basic experiment. *Monthly weather review* **91**(3), 99–164 (1963)
- [33] Freire, D., Cabeza, C., Pauletti, S., Sarasúa, G., Bove, I., Usera, G., Martí, A.C.: Effect of turbulent fluctuations on the behaviour of fountains in stratified environments. In: *Journal of Physics: Conference Series*, vol. 246, p. 012015 (2010). IOP Publishing
- [34] SIS products. https://frostprotection.com/index.php?option=com_content&view=article&id=65&Itemid=189&lang=en-us